1

Fundamentals of Magnetoresistance Effects

Koki Takanashi
Institute for Materials Research, Tohoku University,
Aoba-ku, Sendai, Japan

1.1 Giant Magnetoresistance (GMR) Effect

Giant magnetoresistance (GMR) effect is the most fundamental phenomenon in the field of spintronics. In general, the electric resistance of a material is changed when a magnetic field is applied. This phenomenon is known as a magnetoresistance (MR) effect. Although there are many types of MR effects, the MR effect showing a particularly large resistance change among them is called the GMR effect. However, GMR is different from the conventional MR effects that had been known before, not only quantitatively, but also qualitatively. In 1988, GMR was first reported in the experiment of Fe/Cr superlattices by Fert and his collaborators [1]. That was followed by an enormous amount of studies concerning GMR in nanometer-scaled layered structures containing various kinds of ferromagnetic metals, and GMR was practically used for a read head of a hard disk drive (HDD) in only 10 years after the discovery of GMR. The GMR-based read head had dramatically improved the storage density of HDD until GMR was replaced by tunnel magnetoresistance (TMR) later.

Before the discovery of GMR by Fert *et al.*, the antiferromagnetic coupling of Fe layers through a Cr interlayer had been reported in a trilayer structure consisting of Fe/Cr/Fe by Grünberg and coworkers in 1986 [2]. The antiferromagnetic interlayer exchange coupling is closely related to GMR as more details are shown later. In fact, the MR effect equivalent

Spintronics for Next Generation Innovative Devices, First Edition. Edited by Katsuaki Sato and Eiji Saitoh.

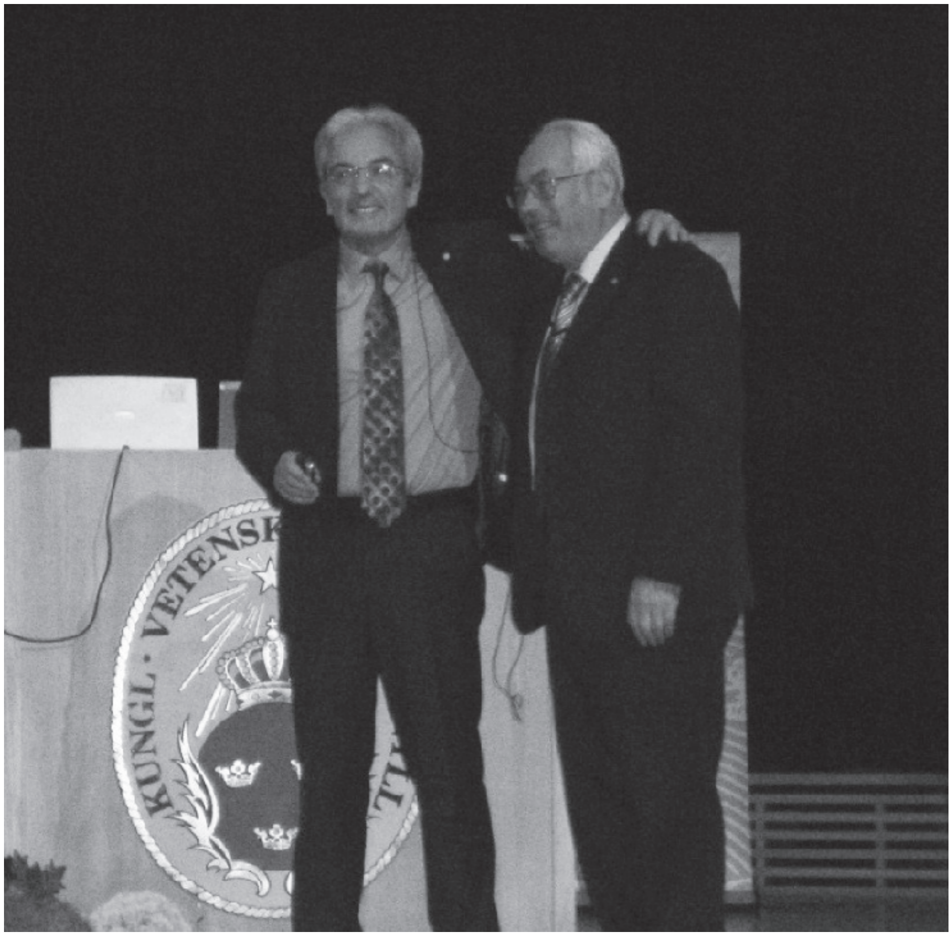

Picture 1.1 *Dr. A. Fert (left) and Dr. P. Günberg shared their joy at the award lecture of 2007 Nobel Prize in Physics*

to GMR, which was smaller than GMR reported by Fert *et al.*, was also observed for the Fe/Cr/Fe trilayer prepared by Grünberg *et al.* [3]. Therefore, both Fert and Grünberg were regarded as the discoverers of GMR, and jointly awarded the Nobel prize in physics in 2007 (Picture 1.1). According to the words by the Nobel Foundation, GMR was considered “the first major application of nanotechnology.” From not only the technological but also physical point of view, as mentioned above, GMR is completely different from the MR known before, and it has brought out a new physical concept, i.e., spin-dependent transport. GMR is the origin for spintronics that is a very popular field now, and without the discovery of GMR no development of spintronics afterward would have appeared.

Section 1.1 starts with a brief explanation of the conventional MR in ferromagnetic materials that had been known before the discovery of GMR. Then the phenomenon, the mechanism and the application of GMR are given. Here, it is noted that the word of GMR means a giant MR effect, and also contains a giant TMR effect[1] (once called the tunnel-type GMR), a CMR (colossal magnetoresistance) effect observed in magnetic oxides, and further different types of giant MR effects in a broad sense. However, GMR normally concerns a giant MR effect observed in "metallic systems" composed of ferromagnetic and nonferromagnetic metals in a nanometer scale. Section 1.1 focuses on the "metallic systems."

1.1.1 Magnetoresistance Effects in Ferromagnetic Materials

All conductive materials, whichever are ferromagnetic or not, exhibit a MR effect. This MR effect is called an ordinary magnetoresistance effect. The electric resistance of a material increases as the applied magnetic field is increased, i.e., the sign of MR is positive. The resistance increase is caused by the Lorentz force that affects the motion of conduction electrons. On the other hand, ferromagnetic materials (including ferrimagnetic materials) with spontaneous magnetization show a characteristic MR effect, which depends on the spontaneous magnetization, and this MR effect is called an anomalous magnetoresistance effect. The anomalous magnetoresistance effect is classified into the following two kinds: an anisotropic magnetoresistance (AMR) effect and a forced effect. In a magnetic field region where magnetic moments are not saturated, the AMR effect appears depending on the relative orientation between magnetization and electric current. The forced effect appears under the application of high magnetic field after saturating the magnetization, and a slight increase in the spontaneous magnetization leads to the corresponding decrease in electric resistance.

The AMR effect, which is well known as a MR in ferromagnetic materials, is usually expressed as

$$\begin{aligned}\rho &= \rho_{\mathrm{l}} \cos^2\theta + \rho_{\mathrm{t}} \cos^2\theta \\ &= \rho_{\mathrm{t}} + (\rho_{\mathrm{l}} - \rho_{\mathrm{t}}) \cos^2\theta, \end{aligned} \tag{1.1}$$

where ρ represents the electric resistivity and θ represents the relative angle between the magnetization vector and the electric current. ρ_{l} and ρ_{t} are the resistances when the magnetization is parallel ($\theta = 0$) and perpendicular ($\theta = \pi/2$) to the electric current, respectively. Generally ρ_{l} is not equal to ρ_{t} ($\rho_{\mathrm{l}} \neq \rho_{\mathrm{t}}$), leading to the appearance of AMR. The origin for AMR is known to be caused by spin–orbit interaction [4] although the details are not shown here.

The magnitude of AMR is defined as the ratio of resistance change (MR ratio: $\Delta\rho/\rho$):

$$\Delta\rho/\rho = (\rho_{\mathrm{l}} - \rho_{\mathrm{t}})/\rho_{\mathrm{av}}, \tag{1.2}$$

where ρ_{av} is the average of the resistance, and is described as

$$\rho_{\mathrm{av}} = \rho_{\mathrm{l}}/3 + 2\rho_{\mathrm{t}}/3 \tag{1.3}$$

by using $\langle \cos^2\theta\rangle_{\mathrm{av}} = 1/3$ and $\langle\sin^2\theta\rangle_{\mathrm{av}} = 2/3$.

[1] Strictly speaking, TMR had been discovered before GMR. However, the effect had been very small at room temperature, and had attracted not much attention from the practical point of view. The discovery of GMR activated the TMR study; leading to the observation of large TMR at room temperature. Based on this historical background, in Section 1.1, GMR is considered to be the origin of spintronics. More details on TMR will be given in Section 1.2.

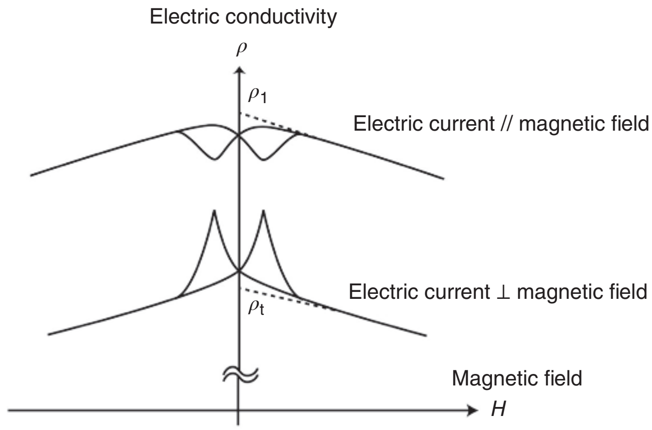

Figure 1.1 *Typical MR curves in a ferromagnetic material. The magnetic field is applied parallel or perpendicular to the direction of electric current*

Figure 1.1 shows a typical MR curve for a ferromagnetic material, where the vertical and horizontal axes represent the electric resistance and the applied magnetic field, respectively. With sweeping the magnetic field from positive to negative and then back to positive again, a hysteresis curve of the resistance shows a maximum or minimum value around the coercivity. The MR curve shown in Figure 1.1 is for the case with $\rho_l > \rho_t$. However, materials with $\rho_l < \rho_t$ also exist. In any case, $\Delta\rho/\rho$ for AMR is usually a small value from 0.1 to a few percent at room temperature [4].

1.1.2 Phenomenon of GMR Effect

The phenomenon of the GMR effect differs from AMR in ferromagnetic materials in terms of both quantitative and qualitative characteristics. First, GMR is isotropic irrespective of the angle between magnetic field and electric current. Second, the resistance decreases remarkably when the magnetization is being saturated, so the sign of MR is negative. A typical GMR curve and the corresponding magnetization curve are shown in Figure 1.2(a) and (b), respectively. The magnitude of GMR is usually defined as the MR ratio ($\Delta\rho/\rho$) and is given by

$$\Delta\rho/\rho = (\rho - \rho_s)/\rho_s, \tag{1.4}$$

where ρ is the maximum resistance around zero magnetic field and ρ_s is the resistance when the magnetization is saturated. Note that in some cases, the change in the resistance ($\Delta\rho = \rho - \rho_s$) is divided by ρ, which leads to a large difference in the MR ratio. In addition, an MR curve showing GMR sometimes contains the contribution of AMR and the difference between ρ_l and ρ_t is observed. However, compared to the total change in the resistance, the AMR effect is rather small and can often be ignored. Since GMR was discovered in Fe/Cr superlattices in 1988 [1], GMR has been reported in various superlattices consisting of ferromagnetic metals (FM) and nonmagnetic metals (NM), such as Co/Cu [5],

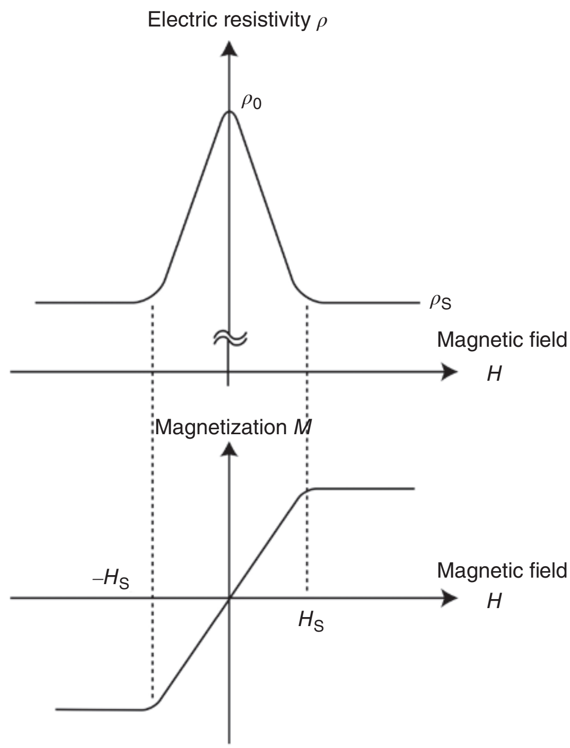

Figure 1.2 *(a) Typical MR curve and (b) magnetization curve of a superlattice showing GMR*

Co/Ag [6], Ni/Ag [7], etc. The superlattice is a thin film composed of two or more different materials, which are alternately deposited in a nanometer scale by thin film preparation methods such as molecular beam epitaxy (MBE) and sputtering.

All the superlattices with any combination of FM and NM do not show GMR. Crucial requirements should be satisfied to show GMR. One requirement is antiferromagnetic interaction between FM layers through a NM layer leading to the antiparallel alignment of magnetization vectors in adjacent FM layers at zero magnetic field. When the magnetic field is applied and increased, the alignment of magnetization turns to parallel which gives rise to the resistance decrease, i.e., the appearance of GMR. Table 1.1 summarizes the reported data in some representative superlattices showing GMR [1, 5–12]. The MR ratios are larger than 10% at room temperature, and reach a few tens to more than 100% at low temperature. GMR in metallic superlattices is caused by spin-dependent scattering of conduction electrons at the interface as mentioned in Section 1.1.3. This effect strongly depends on the condition of the interface, and the GMR is highly sensitive to the structure. Therefore, GMR is not solely determined by the combination of metal elements. Generally, however, we may say that Fe/Cr in Fe-based superlattices and Co/Cu in Co-based superlattices show the largest GMR, which is qualitatively consistent with theoretical calculations [13, 14]. In addition, GMR usually decreases with temperature.

Table 1.1 *GMR effect in various kinds of superlattices*

Superlattices $[A\,(x\,(Å))\,/\,B\,(y\,(Å))_{xN}$	$\Delta\rho/\rho(\%) = (\rho_0 - \rho_s)/\rho_s$	Temperature (K)	Fabrication method	Reference
$[Fe\ (30)/Cr\ (9)]_{\times 30}$	85	4.2	MBE	[1]
$[Fe\ (4.5)/Cr\ (12)]_{\times 50}$	220 42	1.5 300	MBE	[8]
$[Fe\ (20)/Cr\ (12)]_{\times 20}$	33	4.5	Sputtering	[5]
$[Co\ (15)/Cu\ (9)]_{\times 30}$	78 48	4.2 300	Sputtering	[5]
$(Co\ (8)/Cu\ (8.3)]_{\times 60}$	115 65	4.2 295	Sputtering	[10]
$[Fe\ (10.7)/Cu\ (13.7)]_{\times 15}$	26 13	4.2 R.T.	Sputtering	[11]
$[Co\ (6)/Ag\ (25)]_{\times 70}$	38 16	77 R.T.	MBE	[6]
$[Ni\ (8)/Ag\ (11)]_{\times ?}$	26	4.2	Sputtering	[7]
$[Ni_{81}Fe_{19}\ (15)/Cu\ (8)]_{\times 14}$	25 16	4.2 300	Sputtering	[12]

1.1.3 Mechanism of GMR Effect

The mechanism of GMR originates from the spin-dependent scattering of conduction electrons. The spin-dependent scattering occurs in FM layers or at FM/NM interfaces. Here we consider a two-current model where up-spin (↑) and down-spin (↓) electrons pass through two independent channels without taking into account the spin-flip scattering that causes the change of spin orientation. The scattering probability of conduction electrons depends on whether the spin orientation is parallel or antiparallel to the magnetization which is called spin-dependent scattering. The electric resistivity for spins parallel (antiparallel) to the magnetization is written as ρ_+ (ρ_-). Generally $\rho_+ \neq \rho_-$, and here we assume $\rho_+ < \rho_-$. In other words, the electrons with spins parallel to the magnetization have a low scattering possibility while the electrons with spins antiparallel to the magnetization have a high scattering possibility. (Even if we assume the opposite relationship, i.e., $\rho_+ > \rho_-$, there is no influence on the following discussion, keeping the generality.) Figure 1.3 depicts a schematic illustration of the conduction of electrons. In the case of superlattices, the thickness of each layer is of the order of nanometer. Thus the electrons do not stay in one layer during conduction, and flow across the layers even when the electric current is applied in-plane. If the magnetization vectors of adjacent FM layers are parallel, the electrons with ↑ spins parallel to the magnetizations are hardly scattered which contributes dominantly to the conduction, leading to a low electric resistance. On the other hand, if the magnetization vectors are antiparallel, both ↑ spins and ↓ spins should pass through the layers with the opposite magnetization vectors and are significantly scattered, leading to a high electric resistance. In order to discuss the above situation more quantitatively, we consider a

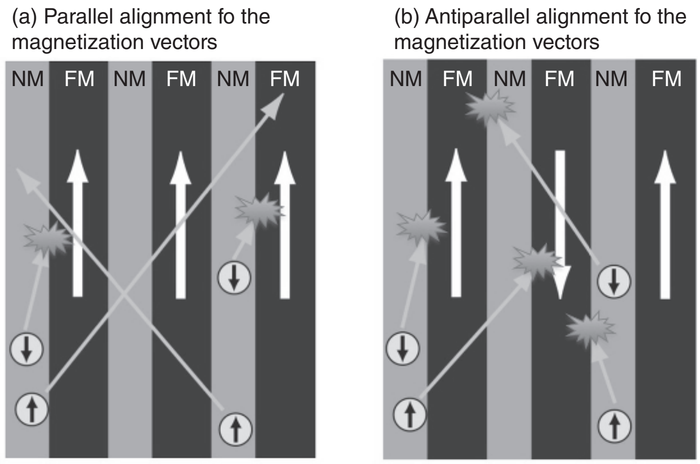

Figure 1.3 *Schematic illustration of the conduction of electrons in a superlattice with alternatively stacked a ferromagnetic metal (FM) and a nonmagnetic metal (NM). The cases for (a) parallel and (b) antiparallel alignments of the magnetization vectors are shown*

parallel circuit of the ↑ spin channel and the ↓ spin channel. Then, the electric resistivity ρ is expressed as

$$1/\rho = 1/\rho_{\uparrow} + 1/\rho_{\downarrow}, \tag{1.5}$$

where $\rho_{\uparrow}$ ($\rho_{\downarrow}$) is the resistivity for the electrons with ↑ (↓) spin. Namely, ρ is rewritten as

$$\rho = \rho_{\uparrow}\rho_{\downarrow}/(\rho_{\uparrow} + \rho_{\downarrow}). \tag{1.6}$$

When all the magnetization vectors are parallel, we consider $\rho_{\uparrow} \sim \rho_{+}$ and $\rho_{\downarrow} \sim \rho_{-}$ and the total resistance ρ_{P} is expressed as

$$\begin{aligned} \rho_P &= \rho_+\rho_-/(\rho_+ + \rho_-) \\ &\sim \rho_+ \quad (\text{for } \rho_+ << \rho_-). \end{aligned} \tag{1.7}$$

When the adjacent magnetization vectors are antiparallel, we consider $\rho_{\uparrow} \sim \rho_{\downarrow} \sim (\rho_+ + \rho_-)/2$, the total resistance ρ_{AP} is expressed as

$$\rho_{\mathrm{AP}} = (\rho_+ + \rho_-)/4. \tag{1.8}$$

With Equations (1.7) and (1.8), the magnitude of GMR is given by

$$\begin{aligned} (\rho_{\mathrm{AP}} - \rho_{\mathrm{P}})/\rho_{\mathrm{P}} &= (\rho_+ - \rho_-)^2/4\rho_+\rho_- \\ &= (1-\alpha)^2/4\alpha, \end{aligned} \tag{1.9}$$

where α is a parameter representing the spin dependence of electron scattering and is defined as

$$\alpha = \rho_-/\rho_+. \tag{1.10}$$

One can see that GMR appears when $\alpha \neq 1$ and GMR is large as $\alpha >> 1$ or $\alpha << 1$.

The requirements for the appearance of GMR are summarized as follows:

(i) Antiparallel alignment of the magnetization vectors in adjacent FM layers through a NM layer.
(ii) Large spin-dependent scattering of electrons ($\alpha >> 1$ or $\alpha << 1$).
(iii) The multilayer period of the superlattice is shorter than the mean free path of conduction electrons.

The first and second requirements have already been mentioned above. The third requirement is an additional one but important as well. If the multilayer period of the superlattice is longer than the mean free path, the electron scattering inside each layer is increased for both ↑ spin and ↓ spin electrons, and the spin-*independent* scattering dominates the total electric resistance, which smears out the difference in the electric resistance between parallel and antiparallel alignments of magnetization vectors.

1.1.4 Oscillatory Behavior of Interlayer Exchange Coupling and GMR

When the antiferromagnetic interlayer exchange coupling acts on FM layers through a NM layer, the saturation field H_s in the MR curve or the magnetization curve where the electric resistance or the magnetization is saturated, is proportional to the exchange coupling energy per unit area J. The antiparallel alignment of magnetization vectors for FM layers requires $J < 0$ (antiferromagnetic coupling), and H_s corresponds to the magnetic field applied to align the magnetization vectors in parallel. The relationship between J and H_s is written as[2]

$$H_s = -4J/M_s \cdot t_{FM} \tag{1.11}$$

where M_s and t_{FM} are the saturation magnetization and the thickness of FM layer, respectively. In the case of $J > 0$ (ferromagnetic coupling), the magnetization vectors of FM layers are aligned in parallel without applied magnetic field, and the magnetization curve shows a simple ferromagnetic behavior ($H_s \sim 0$) and GMR does not appear.

The sign and the magnitude of J depend on the thickness of NM layer, t_{NM}, and have oscillatory behavior as shown in Figure 1.4. Since GMR only appears when $J < 0$, GMR also shows oscillatory behavior. The magnitude of J decreases with t_{NM}, and in general J becomes negligibly small when t_{NM} is larger than several nanometers, leading to the disappearance of GMR. The period of the oscillation in J depends on the material, and is usually a couple of nanometers [9].

As mentioned above, although the interlayer exchange coupling is closely related to GMR, it is important to notice that GMR is in nature a completely separate physical phenomenon. An important point for the appearance of GMR is that the magnetization alignment can be changed from parallel to antiparallel or from antiparallel to parallel by applying the external magnetic field, and there is no direct correlation between GMR and J. In other words, irrespective of the sign and the magnitude of J, if the magnetization alignment is controllable by a certain method, GMR may be observed which is shown in Section 1.1.5. The mechanism of the oscillation in J against t_{NM} was first discussed on the

[2] Technically, Equation (1.11) is valid only for infinite alternation of FM and NM layers. In the case of the trilayer structure FM/NM/FM, the factor is 2 instead of 4.

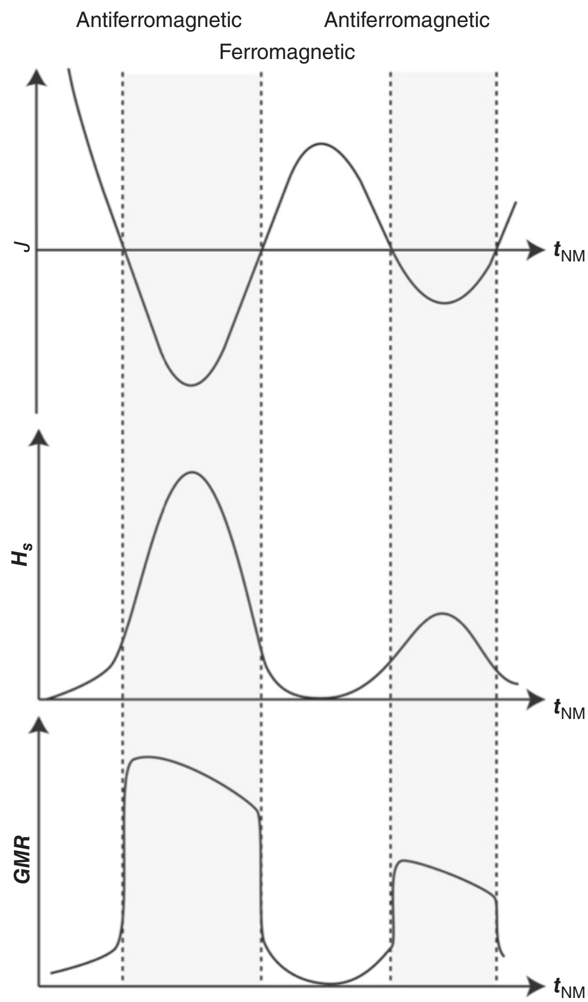

Figure 1.4 *NM layer thickness dependence of exchange coupling energy J of a FM layer through a NM layer, saturation field H_s, and GMR for a superlattice with a FM/NM structure*

basis of the RKKY interaction which successfully explained some part of the oscillatory behavior, but not completely. The phenomena that could not be interpreted only within the framework of RKKY interaction were observed, such as the oscillation in J against the thickness of FM layer t_{FM}. They are now understood by considering the quantum size effect, i.e., the formation of quantum wells caused by the multiple interferences of conduction electrons [15].

1.1.5 The Application of GMR and the Spin Valve

If the strong antiferromagnetic exchange coupling exists between adjacent FM layers, a large external magnetic field is required to align the magnetization vectors in parallel, and

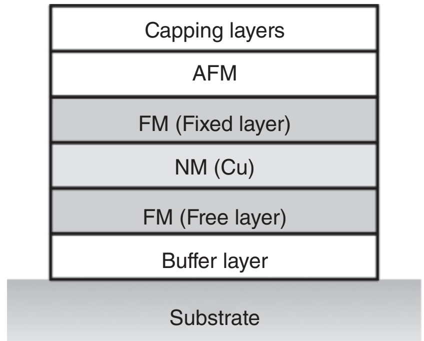

Figure 1.5 *Typical stacking structure of a spin valve*

also to obtain GMR. This was a major obstacle for practical applications of GMR. One possible way to overcome this obstacle is to eliminate the interlayer exchange coupling by increasing the thickness of NM layer and give a difference in coercivities between the adjacent FM layers to achieve the antiparallel alignment of magnetization vectors [16]. Another way is to make a spin-valve structure shown in Figure 1.5 [17]. For the spin-valve structure, one of the two FM layers (free layer) easily changes its magnetization direction with a low magnetic field whereas the other (fixed layer) has its magnetization pinned by the exchange magnetic anisotropy from the neighboring antiferromagnetic layer (AFM). Consequently, GMR appears even under the application of a low external magnetic field. In practical applications, soft magnetic materials like permalloy (Ni−Fe alloy) are usually used as FM layers, Cu is used as a NM layer, while Mn alloys like FeMn, IrMn, PtMn, or oxides like NiO and CoO are used as an AFM layer. The spin-valve structure was used for a read head of HDD in 1998, and played an important role for the remarkable enhancement of recording density as mentioned in the introductory part.

It is noted that the basic structure of a spin valve is the FM/NM/FM trilayer. The magnitude of GMR for superlattices or the MR ratio is known to depend on the number of alternated layers, which means that a structure having more layers shows a larger MR ratio. From the viewpoint of MR ratio, the trilayered structure is unfavorable. In other words, the spin valves realize the high magnetic-field sensitivity at the expense of the MR ratio. In order to improve this point, a five-layered structure of FM/NM/FM/NM/FM with AFM layers on both sides was designed which was called a dual spin valve. However, there is a limitation of the total thickness for the application to ultrahigh density recording. As a result, TMR with the same trilayered structure, showing a high MR ratio compared to GMR, has got to attract more attention, and eventually the TMR read head has replaced the GMR read head in HDD (see Section 1.2.).

1.1.6 CIP-GMR and CPP-GMR

The conventional MR measurement is carried out by measuring the change of the electric resistance under the electric current flow in the film plane. GMR depends on the magnetization configuration of the FM layers. If the electric current flows perpendicularly to the film plane and therefore all the electrons contribute to the conduction through each layer GMR is expected to become larger. The type of GMR when the electric current flows in the film plane is called current-in-plane GMR (CIP-GMR), and when the electric current flows perpendicularly to the film plane, GMR is called current-perpendicular-to-plane GMR (CPP-GMR). Because the thickness of a superlattice is at most several hundred nanometers and the resistance is small due to the metallic conductivity, the measurement of CPP-GMR is not easy. For the measurement of CPP-GMR, various techniques have been developed [18]. Nowadays superlattices are usually microfabricated into a pillar structure with a cross-sectional area of the dimension of micrometer or less, and electrodes are also attached to both the top and bottom ends of the pillar. It has experimentally been confirmed that the MR ratio of CPP-GMR is usually larger than that of CIP-GMR [19].

In the case of CIP-GMR, the mean free path is an important characteristic length as already mentioned in Section 1.1.3. In the case of CPP-GMR, on the other hand, the spin diffusion length (the distance over which the traveling electron spin keeps the initial orientation) is the characteristic length. CPP-GMR is theoretically analyzed by using the Valet–Fert model [20], in which the finite spin diffusion length is taken into account based on the two-current model. By analyzing the experimental data of the layer thickness dependence of CPP-GMR using the Valet–Fert model, the spin dependence in electron scattering is evaluated separately for the bulk and the interface [19].

CPP-GMR was studied from the fundamental point of view at the early stage. Recently, however, it has also attracted much attention in terms of practical applications, because the miniaturization of device elements leads to the increase in the device resistance. In the case of a TMR device for a read head of ultrahigh-density HDD, for example, the resistance of the device becomes so high that it will be difficult to carry out high-speed operation. On the other hand, the resistance of a CPP-GMR device is not so high thanks to all-metal structure. It is to say that the CPP-GMR device will be advantageous because of its low resistance. However, CPP-GMR devices based on the typical FM/NM/FM trilayered structure only showed a small MR ratio around 1% because of a large contribution of parasitic resistance. A variety of studies have been done to increase the MR ratio. From the viewpoint of materials development, half-metallic materials such as Heusler alloys have attracted much attention to improve the MR ratio by applying them to the FM layers, in which the conduction electrons are theoretically predicted to be 100% spin polarized. Co_2MnSi (CMS) is a representative Heusler alloy with high spin polarization, and the large GMR ratios of 36% and 67% at room temperature and 110 K, respectively, were obtained experimentally for the CMS/Ag/CMS stacks [21, 22]. Those experiments stimulated the research activity for CPP-GMR using the Heusler alloys, and recently larger GMR effects have been reported by using Co_2(Fe,Mn)Si [23, 24], and Co_2Fe(Ge,Ga) [25].

1.1.7 GMR in Granular Systems

GMR was observed not only in the layered structure of superlattice, but also in granular systems consisting of ferromagnetic nanoparticles embedded in a nonmagnetic metal matrix. The magnetization vectors of ferromagnetic particles are distributed in random directions under zero external magnetic field because of superparamagnetism caused by thermal fluctuation, or the difference in magnetic anisotropy of each particle. GMR of granular systems appears when the magnetization vectors of particles align to the same direction by applying an external magnetic field.

The granular systems are fabricated with the combination of metal elements with no solid solubility such as Cu–Co [26, 27], Ag–Co [28], Ag–Fe [29], making nonequilibrium solid solution by means of a vapor quenching method such as sputtering, and then giving heat treatment to promote the phase separation. Alternatively, granular systems can also be prepared by only sputtering at a proper substrate temperature. In addition, in the case of systems like Cu–Co which are soluble in the liquid phase, a bulk sample can be obtained by a liquid quenching method [30]. Compared to superlattices, granular systems are easily fabricated. However, low magnetic field sensitivity of MR is a major obstacle for practical applications

1.2 Tunnel Magnetoresistance (TMR) Effect

For a magnetic tunnel junction (MTJ), where two ferromagnetic electrodes are separated by an ultrathin insulating layer, its tunneling probability of electrons depends on the relative orientation of magnetization vectors of two ferromagnetic electrodes. In general, the tunneling probability is high when the magnetization vectors are aligned in parallel, while the tunneling probability is low when the magnetization vectors are aligned in antiparallel. In other words, the electric resistance of MTJ is low (high) for the parallel (antiparallel) alignment of magnetization vectors. This magnetoresistance effect is called a TMR effect.

The research for TMR has a long history. In 1975, Julliére *et al.*. reported a change in the electric resistance by 14% at 4.2 K in an MTJ consisting of Fe/Ge/Co [31]. After that, despite of pioneering work by Maekawa and Gäfvert [32] and Slonczewski [33], a room temperature TMR ratio larger than 10% had not been observed experimentally. In 1995, however, Miyazaki *et al.* [34] and Moodera *et al.* [35] independently reported TMR showing MR ratios larger than 10% at room temperature in a Fe/Al_2O_3/Fe MTJ and a FeCo/Al_2O_3/Co MTJ, respectively. After their discoveries, many experimental studies have been performed, and recently not only for basic scientific interest, but also for practical applications, such as read heads of HDD and magnetic random access memories (MRAMs). In Section 1.2, the principle and the recent progress of TMR studies are reviewed.

1.2.1 The Principle of TMR

Generally TMR arises from the spin polarization of conduction electrons at the Fermi surface for ferromagnetic electrodes. Figure 1.6 shows a schematic illustration for comprehensive explanation of the principle of TMR. With the assumption that the spin-flip scattering is negligible during electron tunneling, the electrons in an up-spin band move to the other up-spin band whereas the electrons in a down-spin band move to the other down-spin band. Therefore, when the numbers of electrons in majority and minority spin bands are different, the tunneling probability depends on the relative orientation of the magnetization vectors

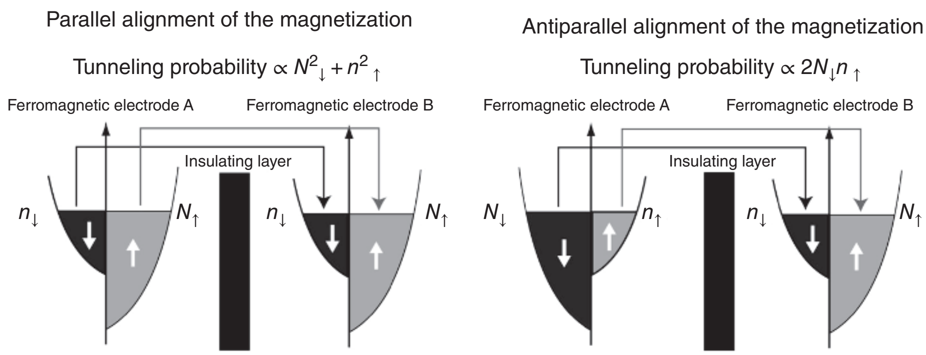

Figure 1.6 *Schematic illustration explaining the principle of TMR.* $n_\downarrow$ ($N_\uparrow$) *represents the density of state at the Fermi level for majority (minority) spins*

for two ferromagnetic electrodes. The relationship between the tunnel conductance G and the relative angle between the two magnetization vectors θ can be expressed as [33]

$$G = G_0(1 + P_1P_2\ \cos\theta), \tag{1.12}$$

where G is the conductance at $\theta = \pi/2$. P_1 and P_2 are the spin polarization factors at the Fermi surfaces of two ferromagnetic electrodes, which are defined as

$$P_{1(2)} = (N_{1(2)} - n_{1(2)})/(N_{1(2)} + n_{1(2)}), \tag{1.13}$$

where $N_{1(2)}$ and $n_{1(2)}$ are the numbers of electrons at the Fermi level in majority and minority spin bands, respectively. Defining R_P and R_AP as the resistances in the cases that the two magnetization vectors are aligned in parallel ($\theta = 0$) and antiparallel ($\theta = \pi$), respectively, the magnitude of TMR can be described as the MR ratio, i.e., the ratio of the resistance difference between R_P and R_AP to R_P. Then, Equation (1.12) yields

$$(R_\mathrm{AP} - R_\mathrm{p})/R_\mathrm{p} = 2P_1P_2/(1 - P_1P_2), \tag{1.14}$$

where $0 \le P_{1(2)} \le 1$. Therefore, high-spin polarization factors of P_1 and P_2 give a large TMR ratio. If the two ferromagnetic electrodes are perfectly spin polarized ($P_1 = P_2 = 1$), R_AP reaches infinity in principle, and the infinite TMR ratio could be obtained.

1.2.2 TMR Effect in Transition Metals and Alloys with Al–O Tunnel Barrier

Many of MTJs studied previously consisted of ferromagnetic transition metals represented by Fe, Co, Ni, and their alloys, which were used as ferromagnetic electrodes, and an Al oxide that was used as an insulating material for the tunneling barrier. Most of the MTJs were prepared using conventional film preparation methods such as sputtering and vacuum evaporation. The films were patterned into a micrometer- or nanometer-sized junction employing a lithography technique, as shown in Figure 1.7. In general, an Al oxide layer for the tunneling barrier was amorphous with nonstoichiometric composition. The Al oxide

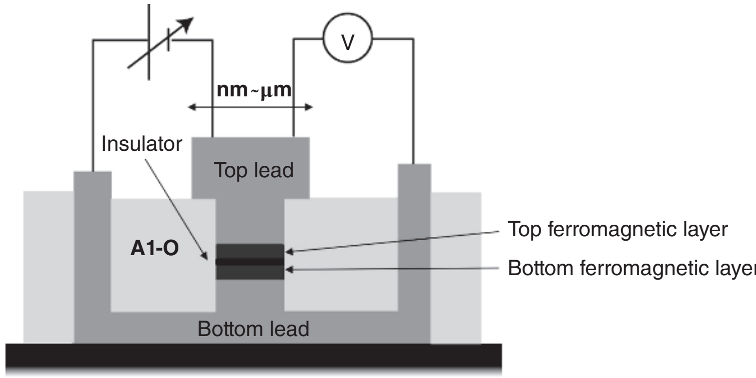

Figure 1.7 *Schematic illustration of the device structure for the measurement of TMR effect*

layer was prepared by depositing a 1–2 nm thick metallic Al film, and then oxidizing the metallic Al film. The oxidization methods are classified roughly into two kinds; one is the oxidization process carried out naturally in an O_2 atmosphere, and the other is the oxidization by using O_2 plasma. Compared to natural oxidization, an Al oxide layer is fabricated quickly by plasma oxidization. However, natural oxidization has a merit in fabricating a MTJ with a low junction resistance.

In the case of MTJ, there is no or quite small interlayer exchange coupling between two ferromagnetic electrodes, which is different from the case of metallic superlattices, and the antiparallel alignment of magnetization vectors cannot be achieved using the interlayer exchange coupling. Therefore, the following methods enable us to achieve the antiparallel orientation of magnetization vectors; making a coercivity difference between two ferromagnetic electrodes by changing the material or the thickness, or fabricating a spin-valve structure with an antiferromagnetic layer.

TMR should be measured carefully because the magnitude of TMR strongly depends on the bias voltage and the measurement temperature. These dependences are mainly attributable to the spin-flip scattering by magnons [36]. In the limit of low bias voltage and low temperature, Equation (1.14) indicates that the TMR ratio depends only on the spin polarization factors of ferromagnetic electrodes in principle. Figure 1.8 shows the plot of representative experimental values of TMR (at low temperature) for the MTJs with the ferromagnetic electrodes of transition metals and their alloys and the Al–O tunneling barrier, versus the calculated values of TMR from Equation (1.14) [37]. There are almost no differences between the experiments and the calculations. The values of spin-polarization factors are obtained independently by employing several methods: (a) preparing a tunnel junction with a target ferromagnetic metal and a superconductor, and measuring its current–voltage characteristics [38, 39], (b) fabricating a point contact with a superconductor, and measuring the Andreev reflection [40], (c) employing spin-polarized photoemission spectroscopy, and so on. The spin-polarization factors shown in the transverse axis of Figure 1.8 correspond to the values obtained with the method (a) using a tunnel junction of the ferromagnetic metal and Al superconductor with an Al oxide barrier. However, the electrons contributing to TMR are sometimes different from the

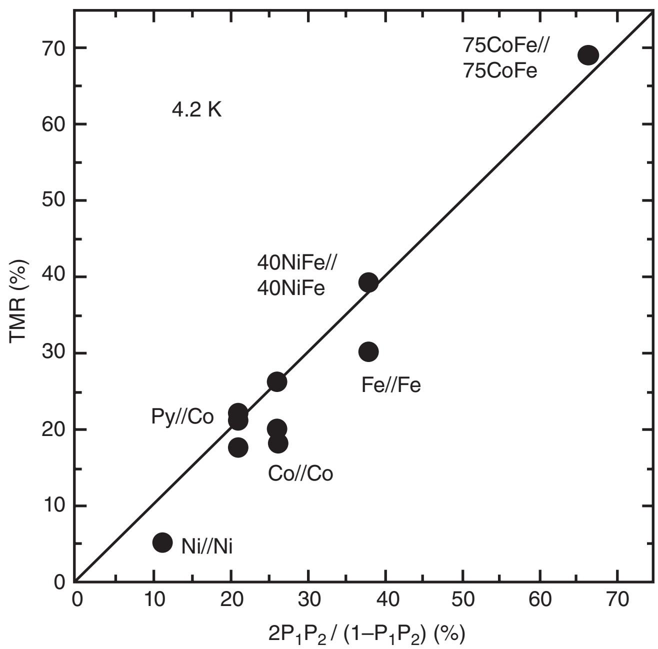

Figure 1.8 *Representative experimental values of TMR ratios obtained at low temperature for the MTJs with the ferromagnetic electrodes of transition metals and their alloys and the Al–O tunneling barrier. The values of TMR calculated from Equation (1.14) are also plotted (Ref. [37])*

electrons related to spin-polarization measurements, and it is noted that the relationship of Equation (1.14) is not always applicable.

1.2.3 TMR Effect in Half-Metallic Systems

As mentioned above, a larger TMR ratio is expected when the spin polarization becomes high, and if a 100% spin-polarized material is used as a ferromagnetic electrode, a huge (infinite in principle) TMR ratio would be obtained. A material with 100% spin polarization is called a half-metal. A half-metal, in other words, has a characteristic band structure in which either majority or minority spin band has an energy gap at the Fermi level. Half-metals are classified roughly into two groups: transition metal oxides and Heusler alloys. The oxide series include Fe_3O_4, CrO_2, and perovskite compounds represented by $LaSrMnO_3$ (LSMO). There is still no report for a large MR ratio for a MTJ with Fe_3O_4 or CrO_2. For the perovskite compounds, a large MR ratio of 1800% was reported at 4.2 K in an MTJ with LSMO/ $SrTiO_3$/LSMO where $SrTiO_3$ (STO) acted as a tunneling barrier [41]. However, LSMO is not suitable for practical application because the Curie temperature is low, and almost no TMR appears at room temperature. In the case of Heusler alloys, there are two types of Heusler alloys: half-Heusler alloys having $C1_b$ structures, and full-Heusler alloys having $L2_1$ structure. NiMnSb is a typical half-Heusler alloy, but a large TMR ratio has not been reported yet. For the full-Heusler alloys, on the other hand, large

TMR effects have been reported. At the early stage of the study on the MTJs with the full-Heusler alloys, the TMR ratios of 20%–40% at room temperature were reported for Co_2MnAl [42], Co_2MnSi [43] and Co_2(Cr, Fe)Al [44] In 2006, the MTJ consisting of Co_2MnSi/Al–O/ Co_2MnSi showed a TMR ratio of 570% at low temperature [45], suggesting the half-metallic feature of Co_2MnSi. Following the experimental demonstration of large TMR effect in the full-Heusler alloy huge TMR ratios were achieved at low temperature for several full-Heusler alloys, e.g., 832% at 9 K for Co_2Fe(Al,Si)/MgO/Co_2Fe(Al,Si) [46], and 1995% at 4.2 K for Co_2MnSi/MgO/Co_2MnSi [47], where the crystalline MgO tunnel barriers were used. The role of MgO barrier is described in Section 1.2. Although the huge TMR effects are obtained at low temperature, the MTJs with full-Heusler alloys show remarkable temperature dependence of the TMR ratio, and it is largely reduced at room temperature [45]. This is a remaining important problem for the full-Heusler alloys.

1.2.4 TMR Effect with Coherent Tunneling

Although Equation (1.14) simply describes the relationship between the TMR and the spin polarization of ferromagnetic electrodes, in realistic cases the relationship between the TMR and the electronic structure is not so simple. If tunneling electrons are scattered strongly at the interface between the electrode and the tunneling barrier, so-called *diffusive limit*, Equation (1.14) well explains the TMR effect by directly using the spin-polarization factor at the interface for each electrode as $P_{1(2)}$. If scattering rates are very small and tunneling electrons travel ballistically, however, the symmetry of wave functions and quantum-mechanical interference affects the TMR significantly.

Yuasa *et al.*, fabricated a MTJ with a single-crystal Fe electrode and an atomically flat Al–O tunneling barrier, and found that the MR ratio was varied for three crystal orientations of (100), (110), and (211). This means that the TMR effect depends on the crystal orientations of ferromagnetic electrodes [48]. It was also revealed that when the thickness of Fe electrodes was smaller than ~ 10 monolayers, the electronic states were modulated by the quantum size effect, and the TMR showed oscillatory behavior due to the formation of quantum well states [49]. Furthermore, for a Co(001)/Cu(001)/Al–O/NiFe MTJ where the nonmagnetic Cu(001) layer was inserted between the Co(001) single crystal electrode and the Al–O tunneling barrier, the TMR ratio showed oscillatory behavior with the sign reversal as a function of the Cu layer thickness [50]. This behavior is attributable to the spin-polarized resonant tunneling via the quantum-well states formed in the Cu interlayer. This cannot be explained only by the spin polarization at the interfaces, but is explained by the quantum-mechanical interference effects, which is called coherent tunneling.

Although an amorphous Al–O layer was used as a tunneling barrier in most cases previously, the TMR effect with coherent tunneling has been found to give rise to a large MR ratio. Since the lattice mismatch between Fe(001) and MgO(001) is very small and Fe(001) grows on MgO(001) epitaxially, this combination is suitable for the fabrication of the epitaxial MTJ. Theoretical calculations also predict a huge TMR ratio of 1000% in a Fe(001)/MgO(001)/Fe(001) MTJ due to a perfectly spin-polarized Δ_1 band of Fe [51, 52]. Yuasa *et al.* fabricated a fully epitaxial Fe(001)/MgO(001)/Fe(001) MTJ, and observed a large MR ratio of ~ 180% at room temperature and over 200% at low temperature [53].

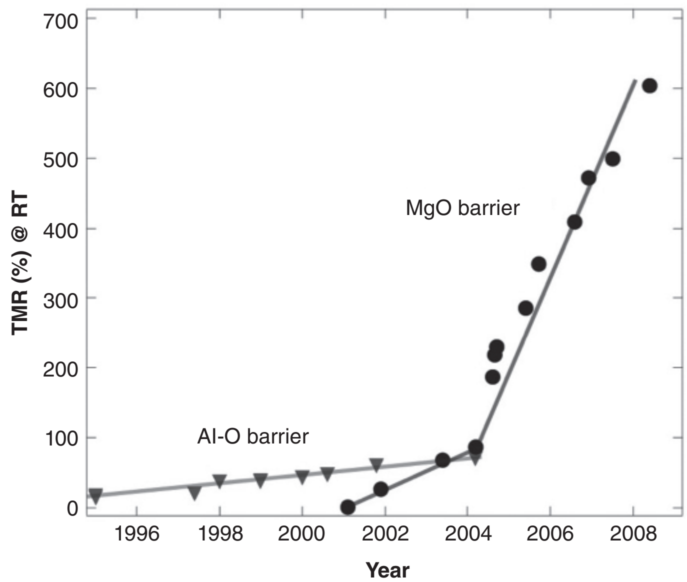

Figure 1.9 *Yearly change of TMR at room temperature with Al–O and MgO tunnel barriers*

They also reported an oscillation of the TMR as a function of the MgO layer thickness due to a coherent effect. Large TMR ratios reaching 200% at room temperature were also observed in a polycrystalline CoFe [54] and an amorphous CoFeB [55], in which the amorphous CoFeB was crystallized into bcc-CoFe by annealing. As in the case of MTJs with Fe/MgO/Fe, the large TMR observed for the CoFe electrode is interpreted within the framework of the coherent tunneling effect. Figure 1.9 shows yearly change in TMR at room temperature with Al–O and MgO tunnel barriers. Huge TMR ratios of 604% and 1144% at room temperature and 5 K, respectively, were obtained for CoFeB/MgO/CoFeB [56].

1.2.5 TMR Effect in Granular Systems

A TMR effect is also observed in granular systems, where magnetic nanoparticles are dispersed in an insulating matrix. If the insulator separating two nanoparticles is thinner than 1–2 nm, electrons move from one particle to another via tunneling. The magnetization vectors for nanoparticles are randomly distributed without magnetic field. When the magnetization vectors are aligned to the same direction by applying an external magnetic field, the tunneling probability of electrons increases, resulting in the decrease of resistance. The phenomenon that the resistance is decreased by the application of magnetic field is the same as that in granular systems with metallic matrices (see Section 1.1.6). However, a characteristic feature for insulating matrices is that the resistance decrease is not caused by spin-dependent scattering but by spin-dependent tunneling. In addition, the magnitudes of electric resistances are quite different. The electric resistances for metallic matrices are of the order of $10–10^2$ $\mu\Omega$ cm; on the other hand, those for insulating matrices are about $10^5–10^6$ $\mu\Omega$ cm (at room temperature). The TMR effects in granular systems are observed in Co, Fe, or CoFe nanoparticles embedded in Al oxide, Si oxide, Mg oxide, rare-earth oxide, or Mg fluoride insulating matrix. For details, see Ref. [57].

References

1. M. N. Baibich, J. M. Broto, A. Fert, *et al*., *Phys. Rev. Lett.*, **61** (1988) 2472.
2. P. Grünberg, R. Schreiber, Y. Pang, *et al*., *Phys. Rev. Lett.*, **57** (1986) 2442.
3. G. Binasch, P. Grünberg, F. Saurenbach, and W. Zinn, *Phys. Rev. B*, **39** (1989) 4828.
4. T. R. McGuire and R. I. Potter, *IEEE Trans. Magn.*, **MAG-11** (1975) 1018.
5. D. H. Mosca, F. Petroff, A. Fert, *et al*., *J. Magn. Magn. Mater.*, **94** (1991) L1.
6. S. Araki, K. Yasui, and Y. Narumiya, *J. Phys. Soc. Jpn.*, **60** (1991) 2827.
7. C. A. dos Santos, B. Rodmacq, M. Vaezzadeh, and B. George, *Appl. Phys. Lett.*, **59** (1991) 126.
8. R. Shad, C. D. Potter, P. Beliën, *et al*., *Appl. Phys. Lett.*, **64** (1994) 3500.
9. S. S. P. Parkin, N. More, and K. P. Roche, *Phys. Rev. Lett.*, **64** (1990) 2304.
10. S. S. P. Parkin, Z. G. Li, and D. J. Smith, *Appl. Phys. Lett.*, **58** (1991) 2710.
11. K. Saito, K. Takanashi, S. Mitani, and H. Fujimori, Technical reports of Institute for Materials Research, Tohoku University, **17** (1997) 55.
12. S. S. P. Parkin, *Appl. Phys. Lett.*, **60** (1992) 2152.
13. J. Inoue, H. Itoh, and S. Maekawa, *J. Phys. Soc. Jpn*, **61** (1992) 1149.
14. H. Itoh, J. Inoue, and S. Maekawa, *Phys. Rev. B*, **47** (1993) 5809.
15. S. N. Okuno and K. Inomata, *Phys. Rev. Lett.*, **72** (1994) 1553
16. T. Shinjo and H. Yamamoto, *J. Phys. Soc. Jpn.*, **59** (1990) 3061.
17. B. Dieny, V. S. Speriosu, S. S. P. Parkin, *et al*., *Phys. Rev. B*, **43** (1991) 1297.
18. *Spin Dependent Transport in Magnetic Nanostructures*, (eds. S. Maekawa and T. Shinjo), p. 29, Taylor & Francis, 2002.
19. For review, J. Bass and W. P. Pratt Jr., *J. Magn. Magn. Mater.*, **200** (1999) 274.
20. T. Valet and A. Fert, *Phys. Rev., B*, **48** (1993) 7099.
21. T. Iwase, Y. Sakuraba, S. Bosu, *et al*., *Appl. Phys. Exp.*, **2** (2009) 063003.
22. Y. Sakuraba, K. Izumi, T. Iwase, *et al*., *Phys. Rev. B*, **82** (2010) 094444.
23. J. Sato, M. Oogane, H. Naganuma, and Y. Ando, *Appl. Phys. Exp.*, **4** (2011) 113005.
24. Y. Sakuraba, M. Ueda, Y. Miura, *et al*., *Appl. Phys. Lett.*, **101** (2012) 252408.
25. Y. K. Takahashi, A. Srinivasan, B. Varaprasad, *et al*., *Appl. Phys. Lett.*, **98** (2011) 152501.
26. A. E. Berkowitz, J. R. Mitchell, M. J. Carey, *et al*., *Phys. Rev. Lett.*, **68** (1992) 3745.
27. J. Q. Xiao, J. S. Jiang, and C. L. Chien, *Phys. Rev. Lett.*, **68** (1992) 3749.
28. J. Q. Xiao, J. S. Jiang, and C. L. Chien, *Phys. Rev., B*, **46** (1992) 9266.
29. A. Tsoukatos, H. Wan, G. C. Hadjipanayis, and Z. G. Li, *Appl. Phys. Lett.*, **61** (1992) 3059.
30. N. Kataoka, H. Endo, K. Fukamichi, and Y. Shimada, *Jpn. J. Appl. Phys.*, **32** (1993) 1969.
31. M. Julliere, *Phys. Lett.*, **54A** (1975) 225.
32. S. Maekawa and U. Gäfvert, *IEEE Trans. Magn.*, **18** (1982) 707.
33. J. C. Slonczewski, *Phys. Rev. B*, **39** (1989) 6995.
34. T. Miyazaki and N. Tezuka, *J. Magn. Magn. Mater.*, **139** (1995) L231.

35. J. S. Moodera, L. R. Kinder, T. M. Wong, and R. Meservey, *Phys. Rev. Lett.*, **74** (1995) 3273.
36. X. F. Han, A. C. C. Yu, M. Oogane, J. Murai, *et al*., *Phys. Rev. B*, **63** (2001) 224404.
37. T. Miyazaki, *J. Mag. Soc. Jpn.*, **25** (2001) 471.
38. R. Meservey and P. M. Tedrow, *Phys. Rep.*, **238** (1994) 173.
39. D. J. Monsma and S. S. P. Parkin, *Appl. Phys. Lett.*, **77** (2000) 720.
40. R. J. Soulen Jr., J. M. Byers, M. S. Osofsky, *et al*., *Science*, **282** (1998) 85.
41. M. Bowen, M. Bibes, A. Barthélémy, *et al*., *Appl. Phys. Lett.*, **82** (2003) 233.
42. H. Kubota, J. Nakata, M. Oogane, *et al*., *Jpn. J. Appl. Phys.*, **43** (2004) L984.
43. A. Hütten, S. Kämmerer, J. Schmalhorst, *et al*., *Phys. Stat. Sol.*, **A201** (2004) 3271.
44. K. Inomata, S. Okamura, R. Goto, and N. Tezuka, *Jpn. J. Appl. Phys.*, **42** (2003) L419.
45. Y. Sakuraba, M. Hattori, M. Oogane, *et al*., *Appl. Phys. Lett.*, **88** (2006) 192508.
46. N. Tezuka, N, Ikeda, F. Mitsuhashi, and S. Sugimoto, *Appl. Phys. Lett.*, **94** (2009) 162504.
47. H. Liu, Y. Honda, T. Taira, *et al*., *Appl. Phys. Lett.*, **101** (2012) 132418.
48. S. Yuasa, T. Sato, E. Tamura, *et al*., *Europhys. Lett.*, **52** (2000) 344.
49. T. Nagahama, S. Yuasa, Y. Suzuki, and E. Tamura, *Appl. Phys. Lett.*, **79** (2001) 4381.
50. S. Yuasa, T. Nagahama, and T. Suzuki, *Science*, **297** (2002) 234.
51. J. Mathon and A. Umerski, *Phys. Rev. B*, **63** (2001) 220403R.
52. W. H. Butler, X.-G. Zhang, T. C. Schulthess, and J. M. Maclaren, *Phys. Rev. B,* **63** (2001) 054416.
53. S. Yuasa, T. Nagahama, A. Fukushima, *et al*., *Nature Mater.*, **3** (2004) 868.
54. S. S. P. Parkin, C. Kaiser, A. Panchula, *et al*., *Nature Mater.*, **3** (2004) 862.
55. D. D. Djayaprawira, K. Tsunekawa, M. Nagai, *et al*., *Appl. Phys. Lett.*, **86** (2005) 092502.
56. S. Ikeda, J. Hayakawa Y. Ashizawa, *et al*., *Appl. Phys. Lett.*, **79** (2001) 4381.
57. H. Fujimori, S. Mitani, and K. Takanashi, *Mater. Sci. Eng. A*, **267** (1999) 184.